

Generative Modeling of Discrete Data Using Geometric Latent Subspaces

Daniel Gonzalez-Alvarado^{1,2,3} Jonas Cassel^{1,4} Stefania Petra^{1,2,3} Christoph Schnörr^{1,3,4}

Abstract

We introduce the use of latent subspaces in the exponential parameter space of product manifolds of categorial distributions, as a tool for learning generative models of discrete data. The low-dimensional latent space encodes statistical dependencies and removes redundant degrees of freedom among the categorial variables. We equip the parameter domain with a Riemannian geometry such that the spaces and distances are related by isometries which enables consistent flow matching. In particular, geodesics become straight lines which makes model training by flow matching effective. Empirical results demonstrate that reduced latent dimensions suffice to represent data for generative modeling.

1. Introduction

Generative models of data constitute a major area of research in machine learning. More recently, generative models of *discrete* (categorical) data and joint probability distributions of discrete random variables have become key aspects of generative modeling (Boll et al., 2024; 2025; Stark et al., 2024; Davis et al., 2024; Cheng et al., 2024; 2025; Williams et al., 2025). Key research topics in this context concern the *representation* of discrete data, either directly or through quantization of real-valued variables, and the *geometry* of the spaces for which these variables and the corresponding probability distributions are defined.

Our **main contribution** in this paper combines *continuous* and *geometric* modeling in a way that is tailored to

- the accurate *encoding and representation* of discrete data,
- the *compression* of *high-dimensional* discrete data, and
- the design of a *generative model* of discrete data.

¹Institute for Mathematics, Heidelberg University ²Mannheim Institute for Intelligent Systems in Medicine, Heidelberg University ³IWR, Heidelberg University ⁴Research Station Geometry and Dynamics, Heidelberg University. Correspondence to: Daniel Gonzalez-Alvarado <daniel.gonzalez@iwr.uni-heidelberg.de>.

To this end, we elaborate the *generalized PCA* approach of classical machine learning (Collins et al., 2001) such that it conforms to the information geometry of discrete joint distributions regarded as statistical manifolds (Amari & Nagaoka, 2000). Regarding the underlying *geometry*, we introduce and propose the Riemannian connection induced by the our e-metric (see Definition 3.1), rather than by the Fisher-Rao metric, in order to relate isometrically the latent subspace and the corresponding induced data manifold, for the consistent representation of discrete data in both domains. We call the resulting major component of our approach *Geometric PCA (GPCA)* latent subspace. One of the consequences of our model is that *geodesics* for training the generative model are *straight lines by geometric construction* which makes flow matching in the low-dimensional latent GPCA subspace particularly computationally efficient.

Figure 1 demonstrates the favorable property of using GPCA for representing *discrete* data, rather than treating such data as points embedded in the ambient Euclidean space. Figure 2 illustrates the components of our approach. Using the *same* dimension of a linear space \mathcal{U} in comparison to basic PCA, a significant subset of the entire discrete data space \mathcal{X} can be represented not only *exactly*, but is also intrinsically *larger* due to the *nonlinear* manifold \mathcal{M} induced in the ambient data space.

We demonstrate empirically on realistic high-dimensional datasets that GPCA achieves significant dimensionality reduction. This highlights the basic manifold assumption of data science and machine learning (Fefferman et al., 2016; Goldt et al., 2020; Meilă & Zhang, 2024), here specifically for *discrete* data and generative models.

Our paper is organized as follows. Section 2 introduces the GPCA. The resulting geometric issues are addressed in Section 3. Section 4 details how the generative model can be trained by flow matching on the GPCA. A more detailed discussion of related work and our contribution is provided in Section 5. Experimental results presented in Section 6 underpin quantitatively our claims.

Frequently used symbols and the basic notation are listed in Appendix A. Mathematical proofs and additional illustrating figures are relegated to Appendices B and C.

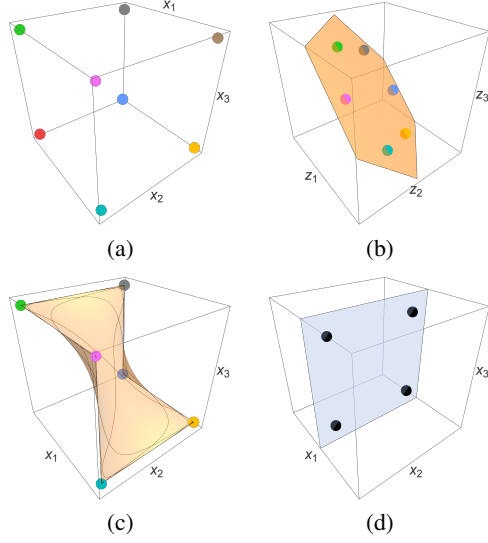


Figure 1. GPCA- vs. PCA-subspaces. (a) The hypercube $\mathcal{X} = \mathbb{H}^3 = \{0, 1\}^3$ as discrete data space. Any $d = 2$ -dimensional affine subspace, when used with linear projection and rounding, can represent at most $2^d = 4$ points exactly. (b) A 2-dimensional geometric latent subspace \mathcal{U} represents $6 > 4$ data points exactly using real latent coordinates. (c) The nonlinear manifold \mathcal{M} induced by the linear GPCA-subspace \mathcal{U} in the data space. (d) Since (a) is isotropic, its covariance is proportional to the identity, so PCA does not reveal a dominant direction. Dropping one coordinate and projection yields the 4 points $\{(1/2, x_2, x_3) : x_2, x_3 \in \{0, 1\}\}$, which are non-integral and do not belong to \mathcal{X} .

2. Discrete Distributions and Geometric PCA

2.1. Discrete Distributions

We consider discrete probability distributions $p \in \Delta_c$ on data taking values in c categories (cf. the notation in Appendix A) and collections of n such data points $x = (x_1, \dots, x_n)^\top \in \mathcal{X}^n$ governed by a joint distribution also denoted by $p \in \Delta_{c^n}$. Points of a training set \mathcal{X}_N^n of size N are denoted by $x_i = (x_{i1}, \dots, x_{in})^\top$, $i \in [N]$. Since for typical sizes of n , p is an intractable large nonnegative tensor, we work with *fully factorized* product distributions

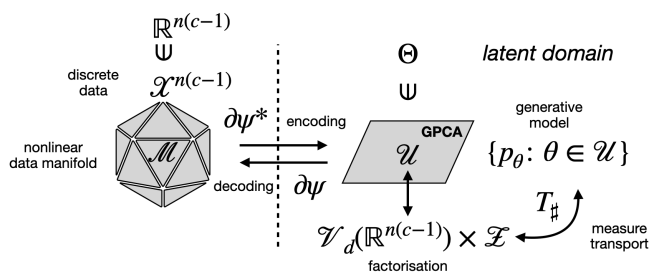


Figure 2. Approach (sketch): Transport of a reference measure on a low-dimensional geometric subspace \mathcal{U} implicitly learns statistical dependencies and a generative model of discrete data, ‘spanned’ after decoding as extreme points of (the closure of) a nonlinear data manifold $\mathcal{M} = \partial\psi(\mathcal{U})$, as illustrated by Figure 1.

$p \in \Delta_c^n = \Delta_c \times \dots \times \Delta_c$ akin to the classical variational mean-field approach (Wainwright & Jordan, 2008), which we, however, restrict to distributions with full support $s = (s_1, \dots, s_n)^\top \in \mathcal{S}_c^n$ and model them as points on a suitable Riemannian manifold (Section 4). Each factor distribution $s_j \in \mathcal{S}_c$ can be turned into the canonical form (Barndorff-Nielsen, 1978; Brown, 1986)

$$s_j = (s_{jl})_{l \in [c]}, \quad s_{jl} = \exp(\langle \theta_j, e_l \rangle - \psi(\theta_j)), \quad (1a)$$

$$\psi(\theta_j) = \log(1 + \langle \mathbb{1}_{c-1}, e^{\theta_j} \rangle), \quad \theta_j \in \mathbb{R}^{c-1}, \quad (1b)$$

uniquely parametrized by $\theta_i \in \mathbb{R}^{c-1}$. Accordingly, $s \in \mathcal{S}_c^n$ is parametrized by $\theta = (\theta_1, \dots, \theta_n)^\top \in \mathbb{R}^{n \times (c-1)}$. We denote by ψ^* the *convex conjugate* of ψ , with the notable property that $\partial\psi^* = (\partial\psi)^{-1}$.

2.2. GPCA and Induced Data Manifolds

We further parametrize product distributions $s \in \mathcal{S}_c^n$ with factors (1) through a latent subspace

$$\mathcal{U} := \text{span}(V) \subset \mathbb{R}^{n(c-1)} \quad (\text{GPCA subspace}) \quad (2)$$

of dimension $d \ll n(c-1)$, spanned by the orthonormal frame $V \in \mathcal{V}_d(\mathbb{R}^{n(c-1)})$ as point on the Stiefel manifold (Edelman et al., 1998) and a latent coefficient vector $z \in \mathcal{Z} := \mathbb{R}^d$ through a low-rank factorization of the vectorized canonical parameter matrix

$$\theta^v = Vz \in \mathcal{U}, \quad V \in \mathcal{V}_d(\mathbb{R}^{n(c-1)}), \quad z \in \mathcal{Z}. \quad (3)$$

The basis vectors $V = (V_1, \dots, V_d)^\top$ are obtained by associating latent coefficient vectors $Z = (Z_1, \dots, Z_N)^\top$ with training data \mathcal{X}_N^n and the approximations

$$\hat{s}_i = \hat{s}_i(VZ_i) = \partial\psi(\hat{\theta}_i), \quad \hat{\theta}_i^v = VZ_i, \quad i \in [N] \quad (4)$$

of each data point $x_i \in \mathcal{X}^n$, and by performing alternating convex minimization of the objective function

$$(V, Z) \mapsto \frac{1}{N} \sum_{i \in [N]} D_{\psi^*}(x_i, \partial\psi(VZ_i)). \quad (5)$$

Here, D_{ψ^*} is the Bregman divergence (Zhang, 2004; Basseville, 2013) generated by the conjugate function ψ^* of the convex Legendre function ψ given by (1b), which acts row-wise in (5). Due to this geometric set-up, we call the resulting latent subspace (2) *Geometric PCA subspace*.

GPCA representation of discrete data: properties.

(1) As illustrated by Figure 1, the map (4) induces a *nonlinear data manifold*

$$\mathcal{M} = \partial\psi(\mathcal{U}), \quad (\text{data manifold}) \quad (6)$$

which, for a fixed subspace dimension d , approximates discrete data much better than applying PCA in the ambient Euclidean space. See Figure 3 and Appendix C.1, Figures 7 and

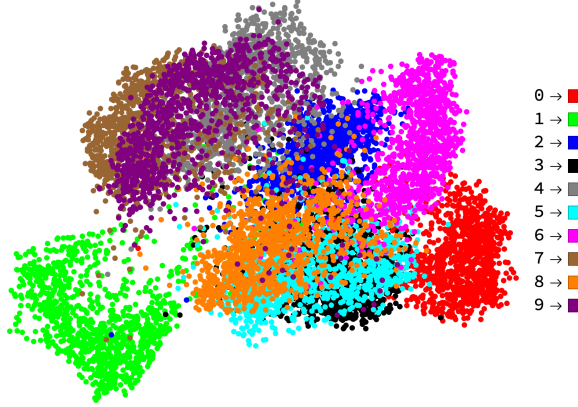


Figure 3. A 2D embedding of the $d = 30$ dimensional latent points $\theta_i = Vz_i \in \mathcal{U}$, $i \in [N]$ corresponding to 10.000 samples $x_i \approx \partial\psi(\theta_i)$ of the MNIST data base (see Figure 7 in Appendix C.1 for a more detailed 3D embedding). This semantically meaningful and *fully unsupervised* embedding of the 4-nearest neighbor graph with nodes θ_i is *purely geometric*: no learning is involved besides determining the GPCA subspace \mathcal{U} . This result underlines the suitability of latent GPCA representations of discrete data, as illustrated by Figure 1. See Figure 8 in Appendix C.1 for a sample of GPCA-based data point approximations.

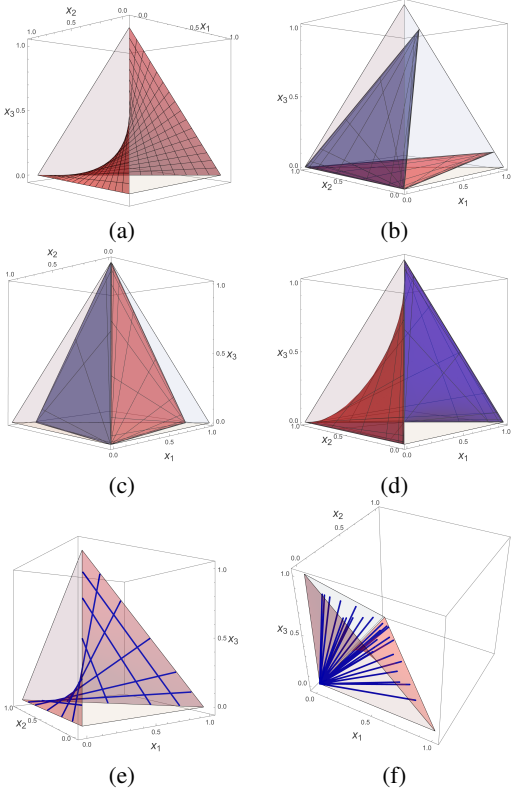


Figure 4. (a) The submanifold of all *factorizing discrete distributions* of two binary variables inside the set of all joint distributions represented as tetrahedron in local coordinates. Examples of foliations of all joint distributions by 2D GPCA subspaces (b)-(d) and by 1D GPCA subspaces (e)-(f). Comparison to (a) shows that learning GPCA subspaces entails *learning statistical dependencies* of discrete random variables.

8, for latent GPCA embeddings and approximations in \mathcal{M} of MNIST data with latent dimension $d = 30 \ll 784 = n$.

(2) Learning GPCA subspaces and data manifolds (6) via (5), together with measure transport (Section 4), entails to *represent and learn statistical dependencies* of discrete random variables. The role of GPCA subspaces in this connection is illustrated by Figure 4.

Distance function, basic assumption. Throughout this paper, we work under the assumption that the discrete data points, can be modeled as samples $s \in \mathcal{S}_c^n$ of a discrete distribution $p \in \mathcal{P}(\mathcal{S}_c^n)$, and p fulfills the ε -GPCA assumption

$$\mathbb{E}_{s \sim p} \left[\|\Pi_{\mathcal{M}} s - s\|_{e,s}^2 \right] \leq \varepsilon, \quad (7)$$

for some $\varepsilon > 0$. Here $\Pi_{\mathcal{M}}$ denotes the Bregman projection of \mathcal{S}_c^n onto $\mathcal{M} \subset \mathcal{S}_c^n$. This shows that the GPCA reconstruction error is within an ε error margin on average.

3. Riemannian Isometries

In the previous sections, we described how to choose low-dimensional subspaces in the space of θ -parameters via the GPCA procedure, parametrized by the z -coordinate system. Our goal now is to express flow matching tasks on the vector subspace \mathcal{U} , which means that we have to equip it with the structure of a manifold in terms of a connection, to comply with the flow matching framework.

We propose the standard Euclidean manifold structure of \mathcal{U} for the connection on \mathcal{U} , induced by the vector space structure of \mathcal{U} . This means that lengths are measured in terms of the Euclidean norm function of $\mathbb{R}^{n \times (c-1)}$, restricted to the subspace \mathcal{U} , and that the tangent space $T_u \mathcal{U}$ is identified with \mathcal{U} . We equip the simplex \mathcal{S}_c^n with a Riemannian metric, defined in terms of the θ -coordinate system on \mathcal{S}_c^n , where the tangent space $T_s \mathcal{S}_c^n$ is identified with $\mathbb{R}^{n \times (c-1)}$.

Definition 3.1 (e -metric). The e -metric g_e on \mathcal{S}_c^n is defined in the θ -coordinate system as the standard scalar product $\langle \cdot, \cdot \rangle$ on the corresponding tangent space. The metric g_e induces a connection on \mathcal{S}_c^n , the Levi-Civita connection corresponding to g_e , which we denote by ∇^e . The simplex \mathcal{S}_c^n thus becomes a Riemannian manifold with respect to g_e and the Riemannian distance function can be explicitly calculated as

$$d_e(s, s') := \|\partial\psi^*(s) - \partial\psi^*(s')\|, \quad \forall s, s' \in \mathcal{S}_c^n, \quad (8)$$

where $\|\cdot\|$ is the Euclidean norm on $\mathbb{R}^{n \times (c-1)}$.

Note that the Christoffel symbols of the connection ∇^e all vanish in the θ -coordinate system, by construction. We can evaluate the metric g_e explicitly for two tangent vectors $\theta, \theta' \in T_s \mathcal{S}_c^n = \mathbb{R}^{n \times (c-1)}$ as the standard scalar product $\theta^\top \theta'$ on $\mathbb{R}^{n \times (c-1)}$, such that the associated norm function

$\|\cdot\|_{e,s}$ on the tangent space in θ -coordinates is the standard norm. The metric can also be evaluated in the alternative representation of tangent vectors $Q \in T_0$, using the canonical identification $T_0 \cong T_s \mathcal{S}_c^n$ induced by the e -coordinates, via the differential

$$d(\partial\psi^*) : \mathcal{S}_c^n \times T_0^n \rightarrow \mathbb{R}^{n \times (c-1)}, \quad (9)$$

$$d(\partial\psi^*)_s(Q) = \left(\frac{Q_{k,i}}{s_{k,i}} - \frac{Q_{k,c}}{s_{k,c}} \right)_{k \in [n], i \in [c-1]}. \quad (10)$$

We denote the induced norm function on T_0 by

$$\|Q\|_{e,s}^2 := \langle d(\partial\psi^*)_s(Q), d(\partial\psi^*)_s(Q) \rangle, \quad (11)$$

This Riemannian structure on \mathcal{S}_c^n captures the e -geometry of the simplex as stated next.

Proposition 3.2 ($\nabla^e = \nabla^1$). *The 1-connection ∇^1 on \mathcal{S}_c^n agrees with the connection ∇^e .*

Remark 3.3 (geodesics). The geodesics of the connection ∇^e are the familiar e -geodesics of information geometry. This shows the relevance of this Riemannian structure of the simplex for flow matching based on e -geodesics, as described in (Boll et al., 2024; 2025). The metric g_e generates the connection ∇^e and thereby the e -geodesics, which are used as the interpolants for flow matching on the simplex.

Proposition 3.4 (isometry relations). *The mapping $\partial\psi : \mathcal{U} \rightarrow \mathcal{S}_c^n$ defines an isometric embedding, when \mathcal{S}_c^n is equipped with the metric g_e . In particular, $\partial\psi$ maps geodesics in \mathcal{U} , i.e. lines of the form $\theta_t = (1-t)\theta_0 + t\theta_1$, to e -geodesics in \mathcal{S}_c^n , which are given by*

$$\phi_t^{(e)} = \phi_t^{(e)}(s_0 | s_1) = \frac{s_0^{1-t} s_1^t}{\langle s_0^{1-t}, s_1^t \rangle}, \quad (c.w.) \quad (12)$$

for $s_0 = \partial\psi(\theta_0)$, $s_1 = \partial\psi(\theta_1)$.

Note that, in particular, the e -geodesics in the induced data manifold \mathcal{M} (cf. Figure 2) lie close to e -geodesics in \mathcal{S}_c^n when the initial and terminal points are close in terms of the Riemannian distance (8).

Proposition 3.5 (geodesic interpolants on \mathcal{M} versus \mathcal{S}_c^n). *Let $s_0, s_1 \in \mathcal{S}_c^n$ and let $\widehat{s}_0, \widehat{s}_1 \in \mathcal{M}$ be latent subspace approximations satisfying*

$$d_e(s_i, \widehat{s}_i) \leq \varepsilon, \quad i = 0, 1, \quad (13)$$

where d_e is the Riemannian distance in (8). Then one also has

$$d_e(\phi_t^{(e)}(s_0 | s_1), \phi_t^{(e)}(\widehat{s}_0 | \widehat{s}_1)) \leq \varepsilon. \quad (14)$$

We refer to Appendix B.1 for the proofs.

4. Flow Matching on \mathcal{U}

The goal of *Flow Matching (FM)* (Lipman et al., 2023; Liu, 2022; Albergo et al., 2023), is to learn a time-dependent vector field which generates a probability path p_t interpolating between a base distribution p_0 and the data distribution p . In the specific case when the data distribution is discrete, several works proposed to work within the simplex geometry, following the Riemannian FM framework (Chen & Lipman, 2024). We adopt this approach but restrict flow matching to the GPCA subspace \mathcal{U} and the induced data manifold \mathcal{M} , respectively (cf. Figure 2).

Specifically, we aim to learn a time-dependent vector field

$$u_t : \mathcal{S}_c^n \rightarrow T_0 \mathcal{S}_c^n, \quad (15)$$

which induces a flow via

$$\frac{d}{dt} \phi_t(s) = u_t(\phi_t(s)), \quad \phi_0(s) = s, \quad (16)$$

and generates the probability path through measure transport $p_t = (\phi_t)_\sharp p_0$ with constraints $p_{t=0} = p_0$ and $p_{t=1} = p$. We note that the base distribution is typically chosen to be a uniform distribution or a transformed Gaussian distribution on the simplex (Stark et al., 2024; Davis et al., 2024; Boll et al., 2024). Additionally, the time horizon can also be extended to \mathbb{R}_+ .

Since neither p_t nor u_t are known in closed form, the FM framework proposes to use interpolants $\phi_t(\cdot | s_1) : \mathcal{S}_c^n \rightarrow \mathcal{S}_c^n$ conditioned on the data samples and to minimize a conditional FM objective, to obtain an approximation of the vector field (15). Working on the simplex endowed with the e -geometry, we set as our primary goal to minimize

$$\mathcal{L}_{\text{CFM}}^{(e)}(w) = \mathbb{E}_{t,s_0,s_1} \left[\|v_t(s_t; w) - \partial_t \phi_t^{(e)}(s_0 | s_1)\|_{e,s_t}^2 \right], \quad (17)$$

with $t \sim \text{unif}(0, 1)$, $s_0 \sim p_0$, $s_1 \sim p_1$ and $\|\cdot\|_{e,s_t}$ being the norm (11) on the tangent space T_0 . To ensure well-defined e -geodesic interpolants $s_t = \phi_t^{(e)}(s_0, s_1)$, data samples $s_1 \sim p$ are translated to the interior of the simplex via a small perturbation. Our choice of conditional interpolants and the Riemannian structure allows the following formulation in *natural* parameters.

Proposition 4.1 (CFM in natural parameters). *The CFM objective (17) is equivalent to*

$$\mathcal{L}_{\text{CFM}}^{(e)}(w) = \mathbb{E}_{t,s_0,s_1} \left[\|v_t^\psi(\theta_t; w) - (\theta_1 - \theta_0)\|^2 \right], \quad (18)$$

where θ_0 and θ_1 are the natural parameters corresponding to s_0 and s_1 , $\theta_t = t\theta_1 + (1-t)\theta_0$, and

$$v_t^\psi(\theta_t; w) := d(\partial\psi^*)_{\partial\psi(\theta_t)}(v_t(\partial\psi(\theta_t); w)). \quad (19)$$

The objective function (18) shows that flow matching with respect to the e -geometry of the simplex is performed via *straight line interpolation* in the space of natural parameters, similarly to the *rectified flow* framework from (Liu, 2022).

Remark 4.2 (e -metric versus Fisher-Rao metric). To the best of our knowledge, *this is the first work* to propose conditional flow matching on the simplex while minimizing a norm defined in the vector space of natural parameters. We note that this is a significant point which distinguishes our approach from existing geometry-based flow matching approaches on the simplex (Davis et al., 2024; Boll et al., 2025): using the e -metric and the associated norm $\|\cdot\|_e$ in favor of the Fisher-Rao metric, due to its compatibility with the e -connection on the simplex. As other authors have pointed out (Boll et al., 2025), the e -connection offers several computational advantages over the metric connection structure induced by the Fisher-Rao metric. For instance, our flow matching objective leverages the *flatness* of the e -connection to simplify the geometric flow matching objective function. In particular, our parametrization allows us to perform most operations relevant to the training process of flow matching models in a *Euclidean vector space*, which speeds up training. The Fisher-Rao metric does not generate the e -connection. Consequently, the e -geodesics used as interpolants in flow matching are not geodesics with respect to the Fisher-Rao metric.

Remark 4.3 (pullback metric on \mathcal{Z}). We note that the mapping $\mathcal{Z} \xrightarrow{V} \mathcal{U} \xrightarrow{\partial\psi} \mathcal{S}_c^n$ allows us to pull back the metric g_e from \mathcal{S}_c^n to \mathcal{Z} . The resulting scalar product on \mathcal{Z} is given by $\langle Vz, Vz' \rangle$, for all z, z' in the tangent bundle $T\mathcal{Z}$. We denote the corresponding norm function by $\|\cdot\|_V$. The CFM objective in \mathcal{Z} then reads

$$\mathcal{L}_{\text{CFM}}^{\mathcal{Z}}(w_z) = \mathbb{E}_{t, z_0, z_1} \left[\|v_t(z_t; w) - (z_1 - z_0)\|_V^2 \right] \quad (20)$$

$$= \mathbb{E}_{t, z_0, z_1} \left[\|Vv_t(z_t; w) - V(z_1 - z_0)\|^2 \right]$$

$$= \mathbb{E}_{t, z_0, z_1} \left[\|Vv_t(z_t; w) - (\hat{\theta}_1 - \hat{\theta}_0)\|^2 \right]. \quad (22)$$

If we choose $p_z = \mathcal{N}(0, I_d)$, then we obtain the same objective as in (18), because the transformed distribution is $V\#p_z = \mathcal{N}(0, V^\top V)$ and likewise was constructed in this form. This allows for significant computational savings through lower-dimensional representations and smaller network architectures, since the optimization can be entirely performed in \mathcal{Z} .

Corollary 4.4 (approximate flow matching). *Let $p_0, p_1 \in \mathcal{P}(\mathcal{S}_c^n)$ denote two probability distributions on \mathcal{S}_c^n and let $\Pi_{\mathcal{M}} : \mathcal{S}_c^n \rightarrow \mathcal{M}$ denote the Bregman projection operator associated to the data manifold \mathcal{M} . If the approximation*

$$\mathbb{E}_{s \sim p_i} \left[\|\Pi_{\mathcal{M}} s - s\|_{e, s}^2 \right] \leq \varepsilon, \quad i = 0, 1 \quad (23)$$

holds for some $\varepsilon > 0$, then one also has

$$\begin{aligned} & \mathbb{E}_{t, s_0, s_1} \left[\|v_t(s_t; w) - \partial_t \phi_t^{(e)}(s_0 | s_1)\|_{e, s_t}^2 \right] \\ & \leq (1 + \sqrt{\varepsilon}) \mathbb{E}_{t, \hat{s}_0, \hat{s}_1} \left[\|v_t(\hat{s}_t; w) - \partial_t \phi_t^{(e)}(\hat{s}_0 | \hat{s}_1)\|_{e, \hat{s}_t}^2 \right] + 4\varepsilon + 4\sqrt{\varepsilon}, \end{aligned} \quad (24)$$

where $t \sim \text{unif}(0, 1)$, $s_0 \sim p_0$, $s_1 \sim p_1$ and $\hat{s}_0 \sim (\Pi_{\mathcal{M}})_\# p_0$, $\hat{s}_1 \sim (\Pi_{\mathcal{M}})_\# p_1$.

Corollary 4.4 and Proposition 4.1 motivate to perform flow matching directly on the latent spaces \mathcal{M} and \mathcal{U} , respectively. Accordingly, we choose as target distribution $\hat{p}_1 = (\Pi_{\mathcal{M}})_\# p_1$, i.e. the Bregman projection of the data distribution p_1 to the GPCA subspace \mathcal{M} . This ensures that the natural parameter approximations $\hat{\theta}$ are located in the subspace \mathcal{M} .

Regarding the assumptions (23), we note that this corresponds to our working hypothesis (7) for the data distribution p_1 . For the reference distribution we choose a normal distribution on the latent space, namely

$$p_0 = (\partial\psi)_\# \mathcal{N}(0, V^\top V). \quad (25)$$

The covariance matrix $V^\top V$ is symmetric and positive semidefinite and ensures that p_0 is only supported on \mathcal{M} . This implies $\hat{p}_0 = (\Pi_{\mathcal{M}})_\# p_0 = p_0$ and ensures that other assumption for p_0 in (23). We argue that in practice the surrogate distribution \hat{p}_1 provides a good approximation of the data distribution p_1 . It is shown empirically in Section 6, cf. Figure 5, that high-dimensional datasets can be represented exactly, in the sense that

$$\sum_{x_i \in \mathcal{X}_N^n} [\|x_i - \text{round}(\partial\psi(Vz_i))\|_1] = 0, \quad (26)$$

which entails significant dimensionality reduction. Furthermore, we demonstrate empirically in Section 6.2 that the assumption of Corollary 4.4 can be fulfilled in different scenarios of practical relevance, such that flow matching can be effectively performed on the low-dimensional GPCA \mathcal{M} -space.

We refer to Appendix B.2 for the proofs.

5. Related Work and Discussion

We distinguish and briefly report

- *prior* related work and, subsequently,
- *recent and current* related work

in order to position our contribution, to point out a current limitation and perspectives.

Prior related work. A major component of our approach, viz. employing *geometric PCA* in the canonical (exponential) parameter space of discrete distributions, has been motivated by a precursor, namely *generalized PCA*, introduced by (Collins et al., 2001).

The basic idea is to regard the squared Euclidean norm, which is used as the objective function for Euclidean data compression in classical principal component analysis (PCA) (Jolliffe, 2002), as a special divergence function (Basseville, 2013) and to replace it with a general Bregman divergence induced by the log-partition function of a regular, minimally represented exponential family of distributions (Brown, 1986), (Barndorff-Nielsen, 1978). From a *geometric* viewpoint, Bregman divergences play a prominent role in the general theory of contrast functions (Matumoto, 1993; Zhang, 2004), in particular in connection with statistical manifolds and information geometry (Lauritzen, 1987; Amari & Nagaoka, 2000; Ay et al., 2017).

Historically, the set-up of GPCA relates through the notion of a ‘link function’ associated with the generalized linear models of classical statistics for regression (McCullagh & Nelder, 1989; Critchley & Salmon, 1994; Warmuth & Kivinen, 2001) and applications to online learning (Kivinen & Warmuth, 1997; Mahony & Williamson, 2001). The gradients of the aforementioned log-partition functions of exponential families of distributions provide a set of canonical link functions.

Our approach elaborates this basic approach

- specifically for joint distributions of *discrete* data in *high* dimensions (Section 2),
- combined with endowing the *latent space* with a *geometry* suited for generative modeling (Section 3).

Recent and current related work. Our paper has been motivated by the *information-geometric* approach of (Boll et al., 2024; 2025) for training generative models of discrete data by flow matching on statistical product manifolds of categorial distributions with full support, equipped with the canonical Fisher-Rao metric and the e-connection of information geometry. This set-up provides a specific novel instance of the general geometric approach (Chen & Lipman, 2024) to flow matching (Lipman et al., 2023; Liu, 2022; Albergo et al., 2023). The recent works (Cheng et al., 2024; 2025) also fall into this category. In addition, the latter paper studies various α -connections besides the e-connection corresponding to $\alpha = 1$. Experimental results indicate that choosing $\alpha = 0.5$ may be beneficial for some applications.

Neither of these works explicitly employ latent subspaces. The authors of (Cheng et al., 2024, pp. 10) point out as limitations (i) that the size of the initial input cannot be modified and, (ii) the “assumption of independence between classes so that the canonical Riemannian structure can be induced by the Fisher metric”.

Our approach addresses these issues in a threefold way: Employing the Geometric PCA subspace

- (a) enables to encode and hence compress discrete data efficiently (Figures 1, Sections 2.2 and 6.1, Appendix C.1),

- (b) enables to represent *non-factorizing* discrete joint distributions (cf. Figure 4) and hence to learn statistical dependencies,

- (c) can be equipped with the natural Riemannian geometry (Section (3)) which isometrically relates spaces and distances.

Regarding *latent space models*, we point out that our encoding map (cf. Figure 2) is *directly* given by information geometry and the geometric representation of discrete joint distributions as statistical manifolds. This stands in contrast to encoder maps that are parametrized and *learned* by a network in more general *non-discrete* scenarios like, e.g., in auto-encoder architectures (Dao et al., 2023; Samaddar et al., 2025). However, despite the *absence* of a *pre-trained* encoding map and hence using *purely geometric* and *unsupervised* latent space embeddings in our approach (in particular, no encoder training is used), the resulting data representations (cf. Figure 3) appear to be natural and semantically meaningful. This underlines that our approach and the geometric set-up is tailored to representing *discrete* data and distributions.

Research on *generative models for discrete* data has become very active recently, e.g. (Boll et al., 2024; 2025; Davis et al., 2024; Cheng et al., 2024; 2025; Williams et al., 2025). We cannot provide a comprehensive review here. The papers by (Boll et al., 2024; 2025; Cheng et al., 2024; 2025) have been addressed above. The latter papers refer to the ‘Dirichlet-flow-matching’ approach introduced in (Davis et al., 2024), which is discussed from the information-geometric point of view in (Boll et al., 2025, Section 3.2.5), to which we kindly refer in view of the limited space.

An interesting *alternative geometric* approach has been proposed recently in the paper (Williams et al., 2025). The authors employ Aitchinson’s geometry known from the sub-area of statistical research concerned with compositional data (Aitchinson, 1982; Filzmoser et al., 2018) and point out as major ingredient of their approach a bijection between the probability simplex and a Euclidean domain, which enables to model and work in the latter space. In this context, we note that information geometry provides a *dually flat structure* for *any* statistical manifold (Amari & Nagaoka, 2000), including the statistical manifold of discrete distributions utilized in our work. The authors of (Williams et al., 2025, Section 5) seem to be aware of this fact, as they point out that “closer inspection of the differences would be highly interesting future work.”

A detailed comparison has been conducted by (Erb & Ay, 2021) who point out the uniqueness of the Fisher information metric regarding invariance properties, the generalization of Euclidean concepts (from squared Euclidean norms to Bregman divergences, the Pythagorean theorem of information geometry, etc.). The authors further point out that these concepts of information geometry have apparently

received only little attention in the field of compositional data analysis and that specific problems of compositional differential calculus naturally follow from information geometry.

Limitation. In connection with flow matching, a major recent research direction concerns the coordination of noise/data pair samples for training the generative model through optimal discrete or semi-discrete transport (e.g. (Pooladian et al., 2023; Tong et al., 2023; Cheng et al., 2025; Mousavi-Hosseini et al., 2025)) which typically improves the experimental performance in comparison with the independent sampling used in the original flow matching approach (Lipman et al., 2023; Chen & Lipman, 2024).

The current research implementation of our approach lacks an OT-based enhancement of flow matching performed in the GPCA subspace, which may partly explain why some benchmark results reported in Section 6 are close to, but not on a par with, the state of the art. Working out a corresponding upgrade of our training procedure is a natural action point for future work.

Perspective. From a *broader* perspective on generative models which also includes deep diffusion models, there seems to emerge currently a confluence of concepts related to such *consistency models* (Albergo et al., 2025; Boffi et al., 2025), which may provide a unifying viewpoint on accelerated generative modeling. A closer inspection of this development and working out the consequences for our *geometric discrete* generative model defines an attractive avenue for future research.

6. Experiments

6.1. Quality of Dimensionality Reduction

Dimensionality reduction via GPCA constitutes the first step of our pipeline, see Figure 2. This step is crucial, as it directly impacts the reconstruction quality of the training data and thereby influences the performance of the subsequent learning stage. Since our approach is driven by the geometry of the latent space induced by GPCA, an insufficient reconstruction quality would lead to a wrong geometric representation. We therefore impose a reconstruction assumption, cf. (7), as a stopping criterion for the GPCA procedure.

We conducted experiments on synthetic toy datasets with many categories $c \gg 2$ (Appendix C.2.1), two common benchmark datasets for discrete data BinarizedMNIST and Cityscapes (LeCun et al., 2010; Cordts et al., 2016) (this section below, Appendices C.1, C.2.2), and two DNA sequence datasets (Section 6.2). Figure 5 reports the reconstruction error measured by the Hamming distance for the MNIST dataset, consisting of 60000 samples of dimension $32 \times 32 \times 2$, and for a downsampled version of Cityscapes

with 2975 training samples of dimension $128 \times 256 \times 8$. Specifically, we evaluated

$$\sum_{i=1}^N d_H(x_i, \text{round}(\partial\psi(Vz_i))) , \quad (27)$$

with $d_H(x, y) = \sum_{j=1}^n \mathbb{1}_{x_j \neq y_j}$, over multiple latent dimensions. We observed that perfect reconstruction, i.e. zero error in Eq. (27), is achieved at comparatively low latent dimensionality: the full Cityscapes training set can be reconstructed using a compression factor of 512, whereas a factor of 51 suffices for BinarizedMNIST. Figures 6 below and Figure 10 (Appendix) display Cityscape labelings for different latent dimensions d . The results show that GPCA reconstructions progressively recover semantically meaningful features as the latent subspace dimension increases. Additional qualitative examples are provided in Appendix C.1.

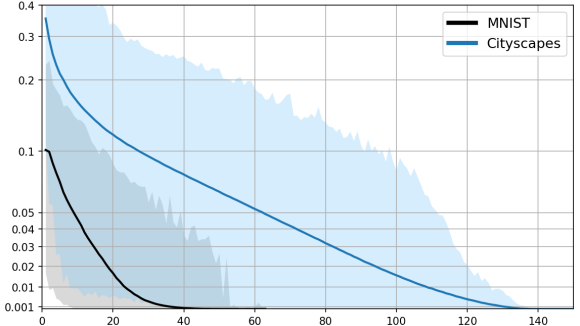


Figure 5. Reconstruction error measured by the Hamming distance (Eq. (27)). The y -axis uses an inverse hyperbolic sine scaling $y' = \sinh^{-1}(y/0.05)$. Shaded regions indicate the minimum and maximum reconstruction errors over the training set.

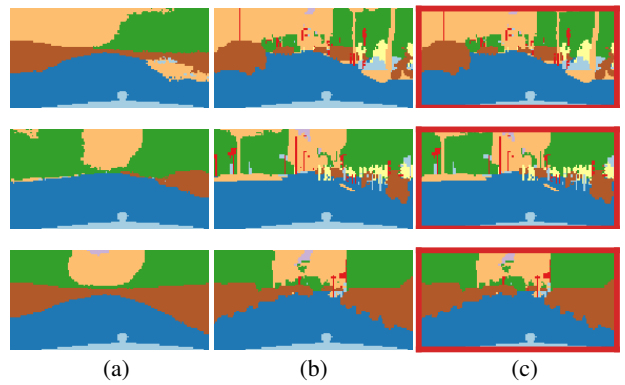


Figure 6. GPCA reconstructions of three Cityscapes samples with latent dimension d : (a) $d = 16$, and (b) $d = 128$, (c) ground-truth input (red).

6.2. Flow Matching Experiments

We tested our GPCA methodology for flow matching for testing DNA data and compared our approach to the geometric flow matching frameworks from (Boll et al., 2025) and (Davis et al., 2024), following closely the experiments from (Stark et al., 2024).

A training set $\mathcal{X}_N \subset \mathcal{S}_c^n$, was used to find a suitable GPCA basis V and coordinates Z by the GPCA procedure described in Section 2. For optimization, we use alternating ADAM gradient descent for V and Z respectively, for a fixed number of 30.000 optimizer steps, followed by constructing the approximate training set $\widehat{\mathcal{X}} \subset \mathcal{M}$ in terms of the coordinates $\theta_i = VZ_i \in \mathcal{U}$ with the property that $\widehat{x}_i = \partial\psi(\theta_i)$ approximates x_i . This approximate training set $\widehat{\mathcal{X}}$ was then used to construct an empirical target and references measures \widehat{p}_1 and \widehat{p}_0 , both supported on \mathcal{M} . Then we trained a neural network via the flow matching objective (18). This approach ensures that the flow matching procedure is confined to the subspace $\mathcal{M} \subset \mathcal{S}_c^n$ and, by virtue of Corollary 4.4, that flow matching with respect to the e -metric for the original dataset \mathcal{X}_N is approximated within an ε -margin, as a consequence of the optimization procedure for determining $\widehat{\mathcal{X}}_N$.

This procedure was applied to the PROMOTER and ENHANCER DNA sequence datasets, following otherwise the methodology of (Avdeyev et al., 2023; Stark et al., 2024; Davis et al., 2024). Table 1 shows the results of the GPCA dimensionality reduction method for these datasets, where we reduced the number of dimensions by a factor of 3. We observe that the different datasets are compressible to varying degrees.

Next we trained flow matching models on these compressed datasets. For validation during training, we performed GPCA-encoding of an unseen validation set \mathcal{X} with the *fixed* basis V , determined from the training set. This yields an approximate validation set, used during training. We used neural networks and hyperparameters as (Davis et al., 2024). Not any kind of tuning of the parameters was done.

Our training results for the ENHANCER experiment listed as Table 2. For the results of the PROMOTER experiment, see Table 3 in Appendix C.2.3. For the ENHANCER sequences, we used the *Fréchet Biological distance (FBD)* from (Stark et al., 2024) to which we refer for more details. The same pretrained models from (Stark et al., 2024) and (Davis et al., 2024) were used for evaluation.¹ ² We observed a slight degradation in test performance when we performed flow

¹As pointed out in (Davis et al., 2024), we are aware that these metrics are somewhat limited as an overall quality estimate for a given model. However, we considered these metrics so as to comply with the common procedures.

²We were not able to reproduce the claimed performance for FISHER-FLOW on the FLY BRAIN dataset, with the instructions from the code repository.

Table 1. Dimensionality reduction results for the ENHANCER DNA sequence datasets. The dimension of all three datasets were reduced by a factor of three. The quality of the dimensional reduction is assessed by evaluating the Hamming distance, normalized by the number of simplices n , between our approximation and the original dataset. We observe that these different dataset allow GPCA compression to different degrees, showing that the datasets exhibit different complexities and corresponding intrinsic dimensionalities.

Dataset	$\dim \mathcal{S}_c^n$	$\dim \mathcal{U}$	normalized Hamming error
MELANOMA	500×3	500	0.01
FLY BRAIN	500×3	500	0.03
PROMOTER	1024×3	1024	0.03

Table 2. Flow matching results for the ENHANCER DNA sequences. We compare our approach using e -geodesics for flow matching, with and without GPCA dimensionality reduction, with the FISHER-FLOW framework. The table lists the mean test performance. We observe that flow matching with e -geodesics is consistent with the FISHER-FLOW method. Despite the data compression, the GPCA reduction causes the performance to degrade only slightly.

METHOD	MELANOMA FBD	FLY BRAIN FBD
LANGUAGE MODEL	35.4	25.2
FISHER-FLOW	29.0	16.9
e -GEODESICS (ours)	31.2	17.0
e -GEODESICS ON \mathcal{M} (ours)	34.6	21.5

matching in terms of e -metric and e -geodesics, compared to the FISHER-FLOW approach. Furthermore, when we work in the approximate data space \mathcal{M} , the test performance slightly degrades further, but remains close to the performance to the other methods, outperforming the Language Model implementation for the ENHANCER test case. Additionally, we observed a slight correlation between the quality of approximation and degradation of test performance. These findings validate our hypothesis to perform flow matching on the lower dimensional \mathcal{U} -space: the approximate data space \mathcal{M} contains enough information and enables sufficient numerical stability to construct generative models on top of it.

7. Conclusion

We introduced a novel generative model based on a geometric latent subspace that induces a nonlinear manifold for representing discrete data. The model enables discrete data compression and efficient model training by flow matching in the lower-dimensional subspace. Our future work will explore consistency models for noise/data samples in the GPCA subspace and the analysis of discrete data via the isometry between the latent and data domains.

Software and Data

Code will be made publicly available.

Acknowledgements

This work is funded by the Deutsche Forschungsgemeinschaft (DFG) under Germany’s Excellence Strategy EXC-2181/1 - 390900948 (the Heidelberg STRUCTURES Excellence Cluster). This work was funded by the Deutsche Forschungsgemeinschaft (DFG), grant SCHA 457/17-2, within the priority programme SPP 2298: Theoretical Foundations of Deep Learning.

References

Aitchinson, J. The Statistical Analysis of Compositional Data. *J. Royal Statistical Soc. B*, 2:139–177, 1982.

Albergo, M., Boffi, N. M., and Vanden-Eijnden, E. Stochastic Interpolants: A Unifying Framework for Flows and Diffusions. *J. Machine Learning Research*, 26(209):1–80, 2025.

Albergo, M. S., Boffi, N. M., and Vanden-Eijnden, E. Stochastic interpolants: A unifying framework for flows and diffusions. *arXiv preprint arXiv:2303.08797*, 2023.

Amari, S.-I. and Nagaoka, H. *Methods of Information Geometry*. Amer. Math. Soc. and Oxford Univ. Press, 2000.

Avdeyev, P., Shi, C., Tan, Y., Dudnyk, K., and Zhou, J. Dirichlet diffusion score model for biological sequence generation. In *International Conference on Machine Learning*, pp. 1276–1301. PMLR, 2023.

Ay, N., Jost, J., Lê, H. V., and Schwachhöfer, L. *Information Geometry*. Springer, 2017.

Barndorff-Nielsen, O. E. *Information and Exponential Families in Statistical Theory*. Wiley, Chichester, 1978.

Basseville, M. Divergence Measures for Statistical Data Processing – An Annotated Bibliography. *Signal Proc.*, 93(4):621–633, 2013.

Boffi, N. M., Albergo, M. S., and Vanden-Eijnden, E. How to Build a Consistency Model: Learning Flow Maps via Self-Distillation. *arXiv:2505.18825*, Oct 5 2025.

Boll, B., Gonzalez-Alvarado, D., and Schnörr, C. Generative Modeling of Discrete Joint Distributions by E-Geodesic Flow Matching on Assignment Manifolds. *arXiv:2402.07846*, 2024.

Boll, B., Gonzalez-Alvarado, D., Petra, S., and Schnörr, C. Generative Assignment Flows for Representing and Learning Joint Distributions of Discrete Data. *J. Math. Imaging Vision*, 67(34), 2025.

Brown, L. D. *Fundamentals of Statistical Exponential Families*. Institute of Mathematical Statistics, Hayward, CA, 1986.

Calin, O. and Udriste, C. *Geometric Modeling in Probability and Statistics*. Springer, 2014.

Chen, R. T. Q. and Lipman, Y. Riemannian Flow Matching on General Geometries. In *ICLR*, 2024.

Cheng, C., Li, J., Peng, J., and Liu, G. Categorical Flow Matching on Statistical Manifolds. *arXiv:2405.16441*, 2024.

Cheng, C., Li, J., Fan, J., and Liu, G. α -Flow: A Unified Framework for Continuous-State Discrete Flow Matching Models. *arXiv:2504.10283*, 2025.

Collins, M., Dasgupta, S., and Schapire, R. E. A Generalization of Principal Component Analysis to the Exponential Family. In *NIPS*, 2001.

Cordts, M., Omran, M., Ramos, S., Rehfeld, T., Enzweiler, M., Benenson, R., Franke, U., Roth, S., and Schiele, B. The Cityscapes Dataset for Semantic Urban Scene Understanding. In *Proceedings of the IEEE Conference on Computer Vision and Pattern Recognition (CVPR)*, 2016.

Critchley, F., Marriott, P., and Salmon, M. Preferred Point Geometry and the Local Differential Geometry of the Kullback-Leibler Divergence. *Ann. Statistics*, 22(3):1587–1602, 1994.

Dao, Q., Phung, H., Nguyen, B., and Tran, A. Flow Matching in Latent Space. *arXiv:2307.08698*, 2023.

Davis, O., Kessler, S., Petrache, M., Ceylan, I. I., Bronstein, M., and Bose, A. J. Fisher Flow Matching for Generative Modeling over Discrete Data. *arXiv:2405.14664*, 2024.

Edelman, A., Arias, T., and Smith, S. The Geometry of Algorithms with Orthogonality Constraints. *SIAM Journal on Matrix Analysis and Applications*, 20(2):303–353, 1998.

Erb, I. and Ay, N. The Information-Geometric Perspectice of Compositional Data Analysis. In Filzmoser, P., Hron, K., Martín-Fernández, J. A., and Palarea-Albaladejo, J. (eds.), *Advances in Compositional Data Analysis*, pp. 21–43. Springer, 2021.

Fefferman, C., Mitter, S., and Narayanan, H. Testing the Manifold Hypothesis. *J. Amer. Math. Soc.*, 29(4):983–1049, 2016.

Filzmoser, P., Hron, K., and Templ, M. *Applied Compositional Data Analysis*. Springer, 2018.

Goldt, S., Mézard, M., Krzakala, F., and Zdeborová, L. Modeling the Influence of Data Structure on Learning in Neural Networks: The Hidden Manifold Model. *Physical Review X*, 10(041044), 2020.

Jolliffe, I. T. *Principal Component Analysis*. Springer, 2nd edition, 2002.

Kivinen, J. and Warmuth, M. Exponentiated Gradient versus Gradient Descent for Linear Predictors. *Inform. Comput.*, 132:1–63, 1997.

Lauritzen, S. L. Chapter 4: Statistical Manifolds. In Gupta, S. S., Amari, S. I., Barndorff-Nielsen, O. E., Kass, R. E., Lauritzen, S. L., and Rao, C. R. (eds.), *Differential Geometry in Statistical Inference*, pp. 163–216. Institute of Mathematical Statistics, Hayward, CA, 1987.

LeCun, Y., Cortes, C., and Burges, C. J. MNIST Handwritten Digit Database. *ATT Labs [Online]*, 2010.

Lipman, Y., Chen, R. T. Q., Ben-Hamu, H., Nickel, M., and Le, M. Flow Matching for Generative Modeling. In *The Eleventh International Conference on Learning Representations*, 2023.

Liu, Q. Rectified flow: A marginal preserving approach to optimal transport. *arXiv preprint arXiv:2209.14577*, 2022.

Mahony, R. E. and Williamson, R. C. Prior Knowledge and Preferential Structures in Gradient Descent Learning Algorithms. *J. Mach. Learning Res.*, 1:311–355, 2001.

Matumoto, T. Any Statistical Manifold has a Contrast Function—on the C^3 -Functions Taking the Minimum at the Diagonal of the Product Manifold. *Hiroshima Math. J.*, 23(2):327–332, 1993.

McCullagh, P. and Nelder, J. *Generalized Linear Models*. Chapman and Hall, 1989.

Meilă, M. and Zhang, H. Manifold Learning: What, How, and Why. *Annual Review of Statistics and Its Application*, 11:393–417, 2024.

Mousavi-Hosseini, A., Zhang, S. Y., Klein, M., and Cuturi, M. Flow Matching with Semidiscrete Couplings. *arXiv:2509.25519*, 2025.

Pooladian, A.-A., Ben-Hamu, H., Domingo-Enrich, C., Amos, B., Lipman, Y., and Chen, R. T. Q. Multisample Flow Matching: Straightening Flows with Minibatch Couplings, 5 2023. *arXiv:2304.14772 [cs]*.

Samaddar, A., Sun, Y., Nilsson, V., and Madireddy, S. Efficient flow matching using latent variables. *arXiv preprint arXiv:2505.04486*, 2025.

Stark, H., Jing, B., Wang, C., Corso, G., Berger, B., Barzilay, R., and Jaakkola, T. Dirichlet Flow Matching with Applications to DNA Sequence Design. *arXiv preprint arXiv:2402.05841*, 2024.

Tong, A., Fatras, K., Malkin, N., Huguet, G., Zhang, Y., Rector-Brooks, J., Wolf, G., and Bengio, Y. Improving and Generalizing Flow-based Generative Models with Minibatch Optimal Transport, 2023. Version Number: 4.

Wainwright, M. and Jordan, M. Graphical Models, Exponential Families, and Variational Inference. *Found. Trends Mach. Learn.*, 1(1-2):1–305, 2008.

Warmuth, M. K. and Kivinen, J. Relative Loss Bounds for Multidimensional Regression Problems. *Machine Learning*, 45:301–329, 2001.

Williams, B., Yeom-Song, V. M., Hartmann, M., and Klami, A. Simplex-to-Euclidean Bijections for Categorical Flow Matching. *arXiv:2510.27480*, 2025.

Zhang, J. Divergence Function, Duality, and Convex Analysis. *Neural Computation*, 16(1):159–195, 2004.

A. Basic Notation

Spaces and particular vectors

$\mathcal{L} := \{1, 2, \dots, c\} =: [c], \quad c \in \mathbb{N}$	label set
$\mathcal{L}^n := [c]^n$	space of discrete data
$\mathcal{X} := \{e_1, \dots, e_c\} \subset \{0, 1\}^c$	one-hot encoding of \mathcal{L}
$\mathcal{X}^n := \mathcal{X} \times \dots \times \mathcal{X}$	one-hot encoding of \mathcal{L}^n
$\mathcal{X}_N^n := \{x_1, \dots, x_N\} \subset \mathcal{X}^n$	given data, training set
$\mathbb{1}_n := (1, 1, \dots, 1)^\top \in \mathbb{R}^n, \quad n \in \mathbb{N}$	constant vector with each component equal to 1
$\Delta_c := \{p \in \mathbb{R}_+^c : \langle \mathbb{1}_c, p \rangle = 1\}$	probability simplex, space of distributions on \mathcal{L}
$\mathcal{S}_c := \text{relint}(\Delta_c) = \{p \in \Delta_c : p_i > 0, \forall i \in [c]\}$	discrete distributions with full support \mathcal{L}
$T_0 := T\mathcal{S}_c = \{v \in \mathbb{R}^c : \langle \mathbb{1}_c, v \rangle = 0\}$	tangent space \mathcal{S}_c in ambient coordinates
$\mathcal{S}_c^n := \mathcal{S}_c \times \dots \times \mathcal{S}_c$	product space of factorizing distributions on \mathcal{L}^n
$T_0^n := T_0 \times \dots \times T_0$	tangent space to \mathcal{S}_c^n in ambient coordinates
$\mathcal{P}(X)$	space of probability distributions supported on a set X

Parametrizations

$\theta_s \in \mathbb{R}^c$: see Equation (1a)	exponential parameters of some distribution $s \in \mathcal{S}_c$
$\psi(\theta_s)$: see Equation (1b)	log-partition function of $s \in \mathcal{S}_c$ corresponding to θ
$\partial\psi$: $\theta_s \mapsto s = \partial\psi(\theta_s) \in \mathcal{S}_c$	decoder map
$\theta_i := (\theta_{i,1}, \dots, \theta_{i,(c-1)})^\top \in \mathbb{R}^{n \times (c-1)}, i \in [N]$	exponential parameters of a close approximation $s_i \approx x_i \in \mathcal{X}_N^n$
$\theta_i^v := \text{vec}_r(\theta_i) \in \mathbb{R}^{n(c-1)}$	vectorization of θ_i by stacking the row vectors
$\partial\psi$: $\theta_i \mapsto s_i = (s_{i,1}, \dots, s_{i,c})^\top \in \mathcal{S}_c^n$	decoder map, defined by factorwise extension
$\partial\psi^* := \partial\psi^{-1} : \mathcal{S}_c \rightarrow \mathbb{R}^{c-1}$	encoder map, convex conjugate function of ψ
$\partial\psi^* : \mathcal{S}_c^n \rightarrow \mathbb{R}^{n \times (c-1)}$	encoder map, defined by factorwise extension

Latent subspace and approximation

d :	latent subspace dimension
$\mathcal{U} := \text{span}(V) \subset \mathbb{R}^{n(c-1)}, V \in \mathbb{R}^{n(c-1) \times d}$	latent subspace spanned by the column vectors of V
$\mathcal{Z} := \mathbb{R}^d$	latent coefficient space
$\mathcal{M} := \partial\psi(\mathcal{U})$ (see Eq. (6))	nonlinear data manifold induced by the latent subspace \mathcal{U}
$\widehat{\theta}_i^v := V z_i \approx \theta_i^v, z_i \in \mathcal{Z}$ (see Eq. (3))	latent subspace approximation
$\widehat{s}_i := \partial\psi(\widehat{\theta}_i) = \partial\psi(\text{vec}_r^{-1}(\widehat{\theta}_i^v)) \in \mathcal{S}_c^n$	latent subspace approximation of s_i
$\widehat{x}_i := \text{round}(\widehat{s}_i) \in \mathcal{X}^n$	latent subspace approximation of the discrete data point x_i

Flow matching and e -geometry

g_e (see Def. 3.1)	e -metric on the simplex
d_e (see Eq. 8)	distance function associated e -metric
$\ \cdot\ _{e, \cdot}$ (see Eq. (11))	e -norm on the tangent space T_0
$\phi^{(e)}$ (see Eq. (12))	e -geodesic flow on the simplex
$u_t : \mathcal{S}_c^n \rightarrow T_0 \mathcal{S}_c^n$ (see Eq. (15))	vector field for flow matching
$v_t(\cdot, w)$	vector field parametrized by the weights w , used to approximation in flow matching
$v_t^\psi(\cdot, w)$ (see Eq. (19))	pushforward of the vector field v_t to the space of natural parameters via ψ

B. Proofs and Additional Details

B.1. Proofs of Section 3

Proof of Proposition 3.2. See Proposition 1.9.1 in (Calin & Udriste, 2014), where it is shown that the 1-connection vanishes in the θ -coordinate system, for any exponential family. This entails $\nabla^e = \nabla^1$, since the two connections are uniquely characterized by the property of vanishing in the θ -coordinate system. \square

Proof of Proposition 3.4. Note that $\partial\psi : \mathcal{U} \rightarrow \mathcal{S}_c^n$ is the restriction of the coordinate chart $\partial\psi : \mathbb{R}^{n \times (c-1)} \rightarrow \mathcal{S}_c^n$ to the subspace \mathcal{U} . We defined the metric g_e by defining the chart $\partial\psi$ as an isometry. Thus, also its restriction is an isometry with the respective induced structures. \square

Proof of Proposition 3.5. First note that since

$$\theta_i = \partial\psi^*(s_i), \quad \hat{\theta}_i = \partial\psi^*(\hat{s}_i), \quad i = 0, 1, \quad (28)$$

the assumption $d_e(s_i, \hat{s}_i) \leq \varepsilon$ implies

$$\|\theta_i - \hat{\theta}_i\| \leq \varepsilon, \quad i = 0, 1. \quad (29)$$

Recall that for the e -geodesic interpolant between s_0 and s_1 we have

$$\partial\psi^*(\phi_t^{(e)}(s_0 \mid s_1)) = (1-t)\partial\psi^*(s_0) + t\partial\psi^*(s_1) = (1-t)\theta_0 + t\theta_1. \quad (30)$$

Therefore, by the triangle inequality, we have

$$d_e(\phi_t^{(e)}(s_0 \mid s_1), \phi_t^{(e)}(\hat{s}_0 \mid \hat{s}_1)) \quad (31)$$

$$= \|\partial\psi^*(\phi_t^{(e)}(s_0 \mid s_1)) - \partial\psi^*(\phi_t^{(e)}(\hat{s}_0 \mid \hat{s}_1))\| \quad (32)$$

$$= \|(1-t)(\theta_0 - \hat{\theta}_0) + t(\theta_1 - \hat{\theta}_1)\| \quad (33)$$

$$\leq (1-t)\|\theta_0 - \hat{\theta}_0\| + t\|\theta_1 - \hat{\theta}_1\| \leq (1-t)\varepsilon + t\varepsilon = \varepsilon. \quad (34)$$

\square

B.2. Proofs of Section 4

Proof of Proposition 4.1. For each $k \in [n]$ the log-ratio (natural) coordinates read

$$\theta_{0,k} = \log \frac{s_{0,k}}{s_{0,k,c}}, \quad \theta_{1,k} = \log \frac{s_{1,k}}{s_{1,k,c}}, \quad (35)$$

and the e -geodesic in theta coordinates is given by the linear interpolation

$$\theta_t = (1-t)\theta_0 + t\theta_1. \quad (36)$$

In particular

$$\partial_t \theta_t = \theta_1 - \theta_0. \quad (37)$$

Since by definition

$$\theta_{t,k} = (\partial\psi^*(s_t))_k = \log \frac{s_{t,k}}{s_{t,c}} = \log s_{t,k} - \log s_{t,c} \mathbb{1}_c, \quad (38)$$

we differentiate and obtain

$$\partial_t \theta_{t,k} = \frac{\partial_t s_{t,k}}{s_{t,k}} - \frac{\partial_t s_{t,c}}{s_{t,c}} \stackrel{(37)}{=} \theta_{1,k} - \theta_{0,k}. \quad (39)$$

In other words we computed

$$d(\partial\psi^*)_{s_t}(s_t) = \theta_1 - \theta_0. \quad (40)$$

We now use the definition of the induced e -norm (11). For any tangent vector $Q \in T_{s_t} \mathcal{S}_c^n$ we have

$$\|Q\|_{e,s_t}^2 = \|d(\partial\psi^*)_{s_t}(Q)\|^2, \quad (41)$$

hence for $Q = v_t(s_t; w) - \partial_t s_t$, we obtain

$$\|v_t(s_t; w) - \partial_t s_t\|_{e,s_t}^2 = \|d(\partial\psi^*)_{s_t}(v_t(s_t; w) - \partial_t s_t)\|^2 \quad (42)$$

$$= \|d(\partial\psi^*)_{s_t}(v_t(s_t; w)) - d(\partial\psi^*)_{s_t}(\partial_t s_t)\|^2 \quad (43)$$

$$\stackrel{(40)}{=} \|d(\partial\psi^*)_{s_t}(v_t(s_t; w)) - (\theta_1 - \theta_0)\|^2. \quad (44)$$

Taking expectations yields concludes the proof. \square

Proof of Corollary 4.4. From Proposition 4.1 we know that

$$\mathbb{E}_{t,s_0,s_1}[\|v_t - \partial_t \phi_t^{(e)}\|_{e,s_t}^2] = \mathbb{E}_{t,\theta_0,\theta_1}[\|v_t^\psi(s_t, w) - (\theta_1 - \theta_0)\|^2], \quad (45)$$

with $v_t^\psi = d(\partial\psi^*)_{s_t}(v_t(s_t; w))$. Furthermore, denoting by $\widehat{\theta}_0$ and $\widehat{\theta}_1$ the natural subspace approximations, we compute

$$\|v_t^\psi(s_t, w) - (\theta_1 - \theta_0)\| = \|v_t^\psi(s_t, w) + (\widehat{\theta}_1 - \widehat{\theta}_0) - (\widehat{\theta}_1 - \widehat{\theta}_0) - (\theta_1 - \theta_0)\| \quad (46a)$$

$$\leq \|v_t^\psi(s_t, w) - (\widehat{\theta}_1 - \widehat{\theta}_0)\| + \|(\widehat{\theta}_1 - \widehat{\theta}_0) - (\theta_1 - \theta_0)\| \quad (46b)$$

$$\leq \|v_t^\psi(s_t, w) - (\widehat{\theta}_1 - \widehat{\theta}_0)\| + \|\widehat{\theta}_1 - \theta_1\| + \|\widehat{\theta}_0 - \theta_0\| \quad (46c)$$

Since for any $\eta > 0$ holds

$$(a + b)^2 \leq (1 + \eta)a^2 + (1 + \frac{1}{\eta})b^2, \quad (47)$$

setting $a = \|v_t^\psi(s_t, w) - (\widehat{\theta}_1 - \widehat{\theta}_0)\|$, $b = \|\widehat{\theta}_1 - \theta_1\| + \|\widehat{\theta}_0 - \theta_0\|$, and $\eta = \sqrt{\varepsilon}$ we obtain

$$\begin{aligned} & \left(\|v_t^\psi(s_t, w) - (\widehat{\theta}_1 - \widehat{\theta}_0)\| + \|\widehat{\theta}_1 - \theta_1\| + \|\widehat{\theta}_0 - \theta_0\| \right)^2 \\ & \leq (1 + \sqrt{\varepsilon})\|v_t^\psi(s_t, w) - (\widehat{\theta}_1 - \widehat{\theta}_0)\|^2 + \left(1 + \frac{1}{\sqrt{\varepsilon}}\right)\left(\|\widehat{\theta}_1 - \theta_1\| + \|\widehat{\theta}_0 - \theta_0\|\right)^2. \end{aligned} \quad (48)$$

Using again (47) with $\eta = 1$ to bound the last term on the r.h.s. yields

$$\begin{aligned} & \left(\|v_t^\psi(s_t, w) - (\widehat{\theta}_1 - \widehat{\theta}_0)\| + \|\widehat{\theta}_1 - \theta_1\| + \|\widehat{\theta}_0 - \theta_0\| \right)^2 \\ & \leq (1 + \sqrt{\varepsilon})\|v_t^\psi(s_t, w) - (\widehat{\theta}_1 - \widehat{\theta}_0)\|^2 + \left(1 + \frac{1}{\sqrt{\varepsilon}}\right)\left(2\|\widehat{\theta}_1 - \theta_1\|^2 + 2\|\widehat{\theta}_0 - \theta_0\|^2\right). \end{aligned} \quad (49)$$

Hence, by squaring and taking expectations on both sides of (46), and using our assumption (7) we get

$$\mathbb{E}_{t,\theta_0,\theta_1}[\|v_t^\psi(s_t, w) - (\theta_1 - \theta_0)\|^2] \leq \mathbb{E}_{t,\theta_0,\theta_1}\left[(1 + \sqrt{\varepsilon})\|v_t^\psi(s_t, w) - (\widehat{\theta}_1 - \widehat{\theta}_0)\|^2\right] + \left(1 + \frac{1}{\sqrt{\varepsilon}}\right)(2\varepsilon + 2\varepsilon) \quad (50)$$

$$= (1 + \sqrt{\varepsilon})\mathbb{E}_{t,\theta_0,\theta_1}[\|v_t^\psi(s_t, w) - (\widehat{\theta}_1 - \widehat{\theta}_0)\|^2] + 4\varepsilon + 4\sqrt{\varepsilon}. \quad (51)$$

\square

C. Additional Experiments and Experimental Details

C.1. Additional GPCA Experiments

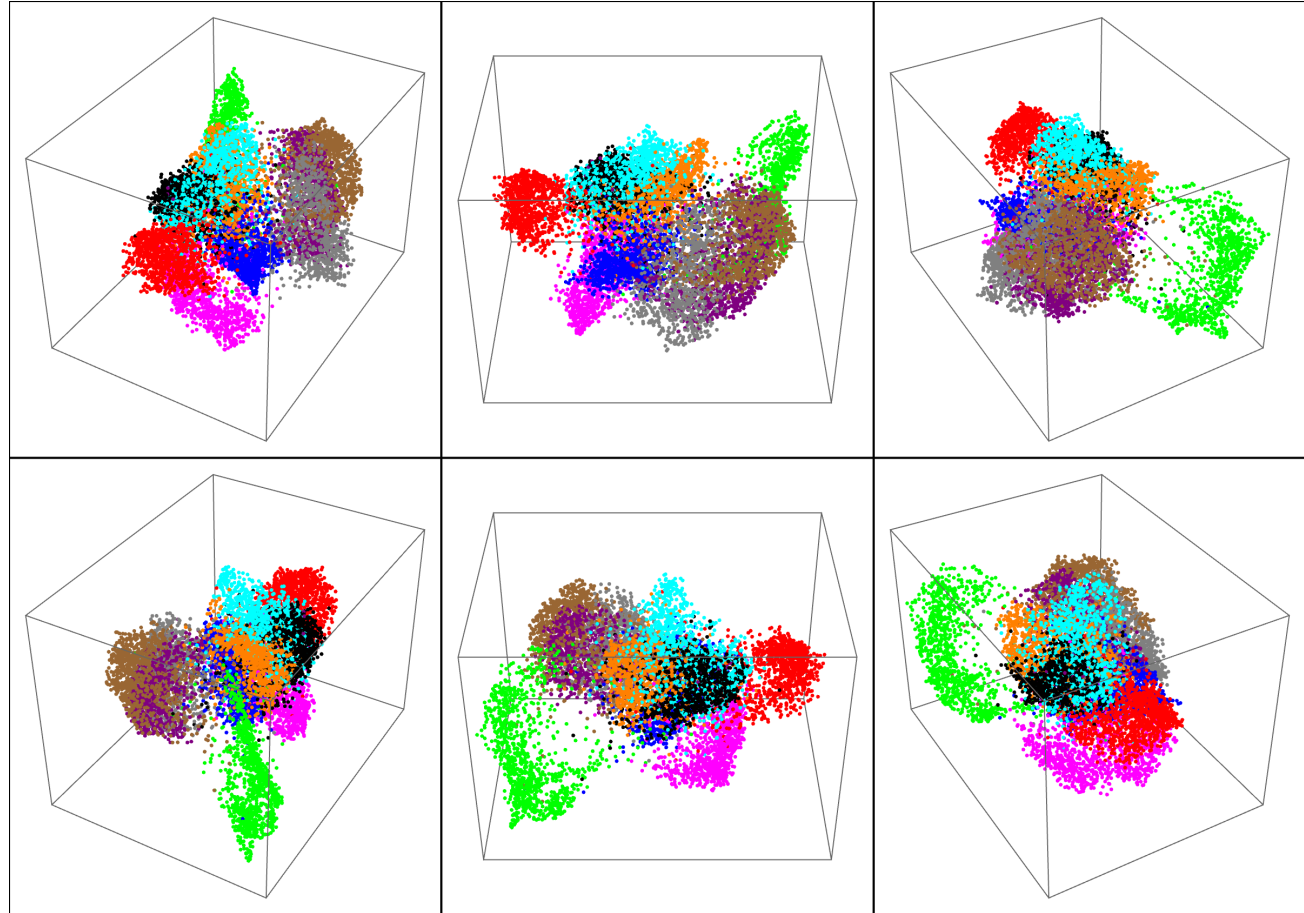


Figure 7. A more detailed 3D embedding of the 30-dimensional latent data points representing a corresponding sample from the MNIST data base. We refer to the further comments in the caption of Figure 3.



Figure 8. Latent space approximations. A random sample of MNIST data points x_i and their GPCA-based approximations $\hat{x}_i = \partial\psi(\theta_i)$. The vast majority of MNIST digits $x_i \in \{0, 1\}^{784}$ can be accurately approximated using a fixed 30-dimensional latent GPCA-subspace \mathcal{U} . The alternatingly colored rows display randomly selected MNIST digits x_i (framed with gray) and their approximations \hat{x}_i (framed with green).

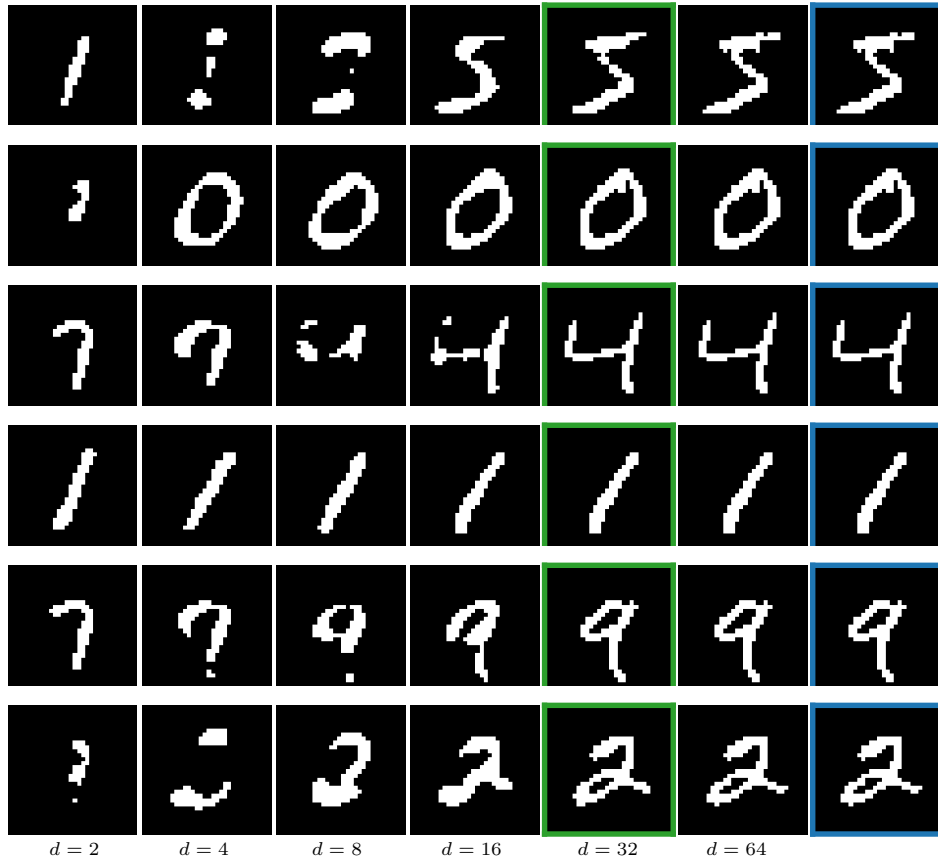


Figure 9. GPCA data reconstructions for varying dimensions. The rightmost column shows MNIST data samples $x_i \in \mathcal{X}_N^n$ (marked in blue). From **left to right:** reconstructions $\hat{x}_i = \text{round}(\partial\psi(\theta_i))$ corresponding to compression factors 1024, 512, 256, 128, 64 and 32 respectively. The reconstruction highlighted in green indicates the GPCA setting used in practice.

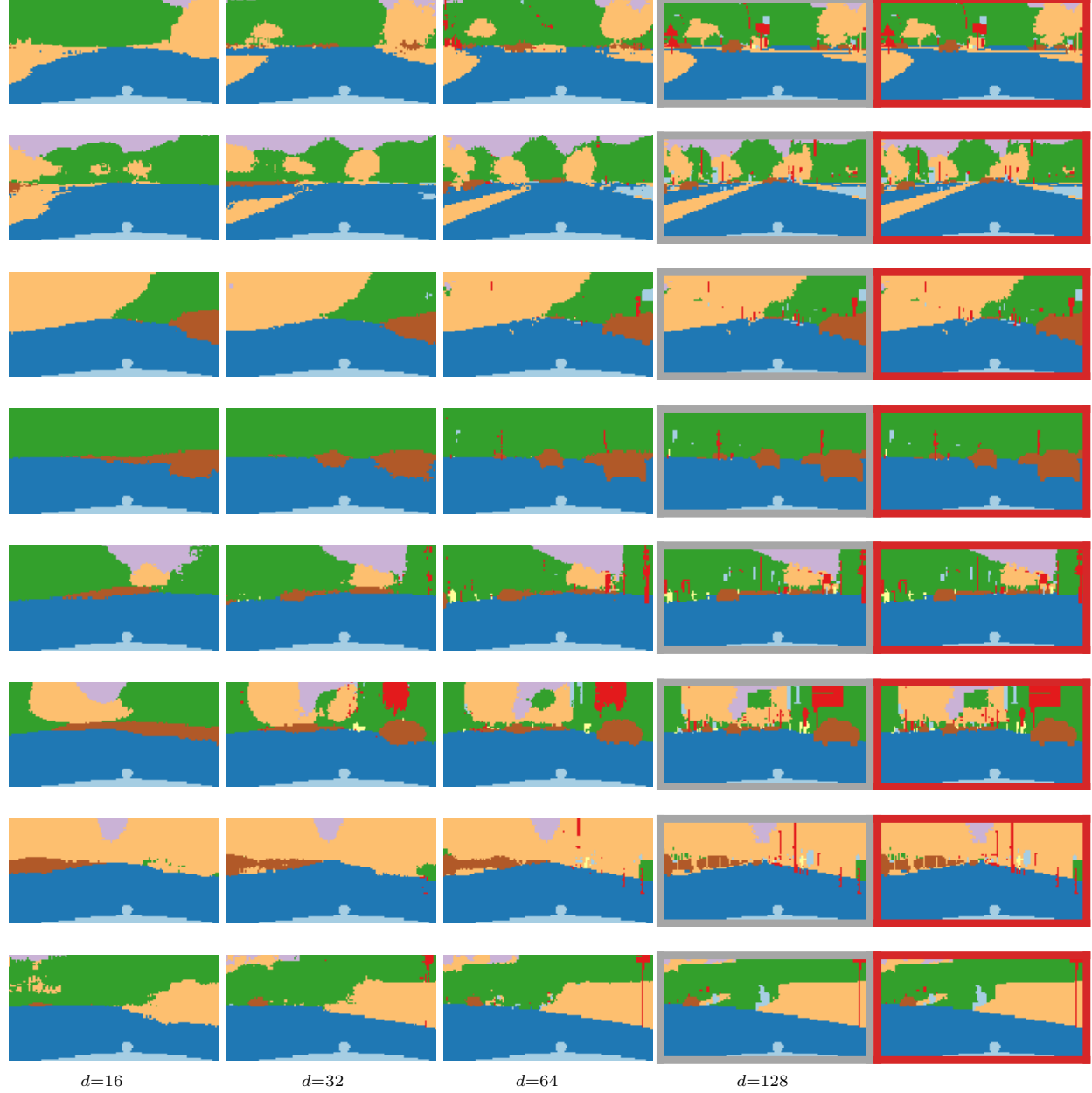


Figure 10. GPCA data reconstructions for varying dimensions. The rightmost column shows Cityscapes data samples $x_i \in \mathcal{X}_N^n$ (marked in red). From **left to right**: reconstructions $\hat{x}_i = \text{round}(\partial\psi(\theta_i))$ corresponding to compression factors 4096, 2048, 1024, and 512, respectively. The reconstruction highlighted in gray indicates the GPCA setting used in practice.

C.2. Additional Flow Matching Experiments

C.2.1. TOY DATASETS

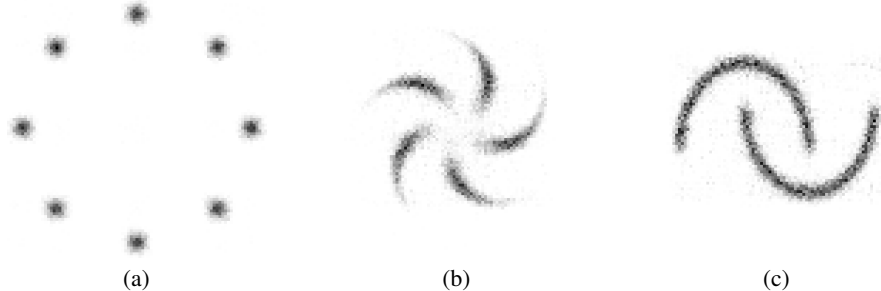


Figure 11. Empirical joint distributions of samples generated by our generative model described in Section 4. The learned distributions (a) Gaussian mixture, (b) pinwheel, and (c) two moons, are *discrete* distributions over $c = 92$ categories of $n = 2$ variables. The figures show empirical distributions estimated from $N = 10.000$ samples, obtained by evaluating the generative model using a latent dimension $d = 16$.

C.2.2. MNIST

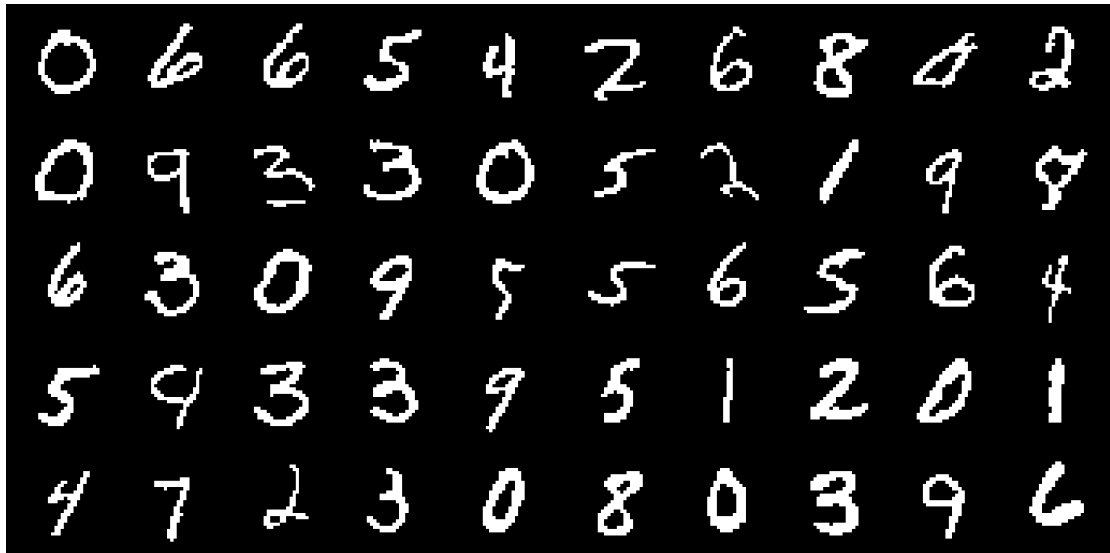


Figure 12. MNIST samples generated by our generative model described in Section 4 using a GPCA latent dimension of $d = 64$.

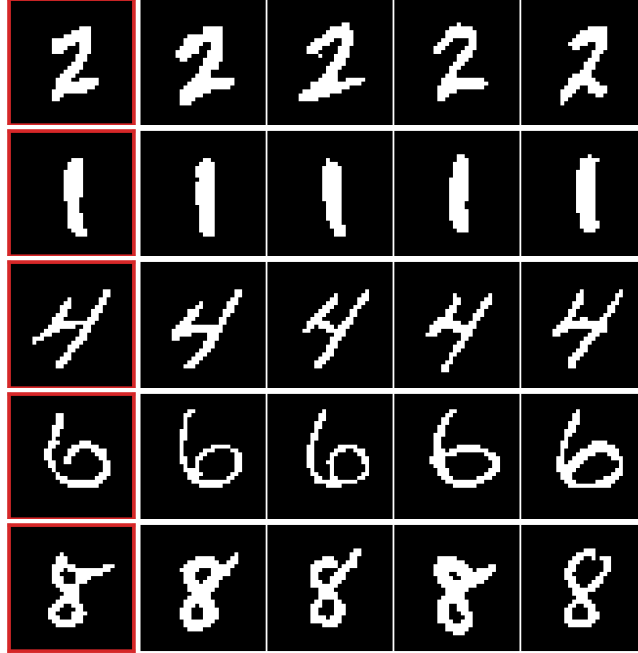


Figure 13. Comparison of model-generated and data samples. The leftmost column (marked red) shows samples generated by our model (Section 4) using a GPCA latent dimension of $d = 64$. The remaining panels depict the five closest training samples in terms of Hamming distance. This figure illustrates the model’s ability to generate novel data.

C.2.3. PROMOTER

We report here the training results from Section 6.2 for the ENHANCER DNA sequence data. The test metric that we used for PROMOTER sequences is the mean squared error method, based on the SEI-model, as described in (Stark et al., 2024).

Table 3. Flow matching results for the PROMOTER DNA sequences. We compare our approach using e -geodesics for flow matching, with and without GPCA dimensionality reduction, with the FISHER-FLOW framework. The table lists the mean test performance. We observe that flow matching with e -geodesics is consistent with the FISHER-FLOW method, whereas here GPCA reduction causes the performance to degrade more severely than for the ENHANCER sequences. This shows that the intrinsic complexity of the data determines the potential for GPCA-based data compression.

METHOD	SEI-MSE
LANGUAGE MODEL	0.034
FISHER-FLOW	0.029
e -GEODESICS (ours)	0.029
e -GEODESICS ON \mathcal{M} (ours)	0.038